九州大学大学院総合理工学府報告
第 43 巻 第 2 号 11-23 頁 令和 4 年 2 月

Engineering Sciences Reports, Kyushu University
Vol. 43, No. 2, pp. 11-23, FEB, 2022

Formation of Excited CH($A^2\Delta$) and CD($A^2\Delta$) Radicals by Collisions of Metastable Ar($^3P_2$) Atoms with C_2H, C_2D, and C_2H_3 Radicals in an Ar Flowing Afterglow

Masaharu TSUJI[*1,2†] Takahiro KOMATSU[*3] Keiko UTO[*1]
Jun-Ichiro HAYASHI[*1,2] and Takeshi TSUJI[*4]
[†]E-mail of corresponding author: tsuji@cm.kyushu-u.ac.jp

(Received November 9, 2021, accepted November 24, 2021)

CH($A^2\Delta$–$X^2\Pi_r$) and CD($A^2\Delta$–$X^2\Pi_r$) emission systems have been observed by dissociative excitation of C_2H, C_2D, and C_2H_3 radicals by collisions with metastable Ar($^3P_2$:11.55 eV) atoms in the Ar flowing afterglow. C_2H, C_2D, and C_2H_3 radicals were generated by the reactions of F atoms with C_2H_2, C_2D_2, and C_2H_4, respectively. The nascent vibrational and rotational distributions of CH(A:v'=0–2) and CD(A: v' =0–2) were determined from computer simulation of observed emission spectra. The vibrational distributions of CH(A) and CD(A) rapidly decreased with increasing v' in all three reactions. The rotational distributions of CH(A:v'=0–2) and CD(A:v'=0–2) states were expressed by single Boltzmann temperatures of 300–1900 K and 600–3800 K, respectively. High rotational excitation of CH(A) and CD(A) in the Ar($^3P_2$)/C_2H and Ar($^3P_2$)/C_2D reactions suggested that bending modes of precursor C_2H** and C_2D** Rydberg states are excited. The observed rovibrational distributions of CH(A) and CD(A) in the Ar($^3P_2$)/C_2H and Ar($^3P_2$)/C_2D reactions indicated that most of excess energies are deposited into relative translational energies of CH(A) + C and CD(A) + C products. The observed vibrational and rotational distributions were compared with statistical prior ones for characterizing dynamical features of reactions.

Key words: *Dissociative excitation, Aliphatic hydrocarbon radicals, Metastable Ar* atoms, Flowing afterglow, Energy transfer, Rovibrational distribution, Statistic dissociation models, Rydberg state*

1. Introduction

The chemical vapor deposition of such simple aliphatic hydrocarbons as CH_4 and C_2H_2 in a plasma reactor has been widely used for making carbon films.[1-3] In general, hydrocarbons are diluted by a rare gas and H_2 to maintain stable plasma. This caused increased interest in studies on dissociation processes of aliphatic hydrocarbons diluted by rare gases in the plasma reactor. We have made systematic studies on dissociative excitation of simple aliphatic hydrocarbons by collisions with the metastable Kr($^3P_2$), Ar($^3P_2$), Ne($^3P_{0,2}$), and He(2^3S) atoms in the flowing afterglow (FA).[4-8] Product state distributions were obtained by analyzing the emission spectra.

As part of the continuing research program to investigate the energy-transfer processes between metastable rare gas atoms and simple aliphatic hydrocarbons, we have previously extended this study to the reactions of Xe($^3P_2$), Kr($^3P_2$), and Ar($^3P_2$) with CH_3 and C_2H_5 radicals, which are the simplest alkyl radicals.[9,10] The excited CH(A,B) states were formed as dominant emitting exit channels. The rovibrational distributions were determined by a spectral simulation. These distributions were compared with the results from statistical model calculations for characterizing the dynamical features of the reactions.

In the present study, emission spectra resulting from energy-transfer reactions of Ar($^3P_2$) atoms with C_2H, C_2D, and C_2H_3 radicals are measured in the FA. The rovibrational distributions of CH(A) and CD(A) are determined by a computer simulation of observed band profiles. The observed

*1 Institute for Materials Chemistry and Engineering, and Research and Education Center of Green Technology
*2 Department of Applied Science for Electronics and Materials
*3 Department of Applied Science for Electronics and Materials, Graduate Student
*4 Department of Materials Science, Shimane University

rovibrational distributions are compared with those from statistical two-body and three-body dissociation models to characterize the dynamical features of the reactions. On the basis of these data, energy-transfer mechanisms are discussed.

2. Experimental

Figure 1 shows a schematic diagram of the FA apparatus used in the present study. This flowing system was evacuated continuously with a 10000 *l*/min mechanical booster pump (ULVAC 006) backed by a 1600 *l*/min oil rotary pump. The following gases were used in this study: Ar (Nippon Sanso: purity: 99.9999%), C_2H_2 (Eto Sanso: 99.0%), C_2H_4 (Eto Sanso: 99.0%), C_2H_6 (Eto Sanso: 99.0%), and CF_4 (Seitetsu Kagaku: 99.5%). C_2D_2 was synthesized by the reaction of CaC_2 with D_2O as reported in our previous paper.[7)]

There are two microwave (MW) discharge sources, which are denoted as MW(A) and MW(B) in Fig. 1. MW(A) was used for the generation of F atoms by MW discharge of Ar/CF_4 mixture. MW(B) was used for the generation of metastable Ar($^3P_2$: 11.55 eV, $^3P_0$: 11.72 eV) atoms. Since the [Ar($^3P_0$)]/[Ar($^3P_2$)] ratio has been reported to be about 0.01,[11)] the contribution of the upper Ar($^3P_0$) spin-orbit component could be negligible in our condition.

The C_2H, C_2D, and C_2H_3 radicals were generated by the following hydrogen abstraction reaction by F atoms:[12,13)]

$$F + C_2H_2 \rightarrow C_2H + H \quad (1)$$
$$F + C_2D_2 \rightarrow C_2D + D \quad (2)$$
$$F + C_2H_4 \rightarrow C_2H_3 + H \quad (3)$$

where fluorine atoms were produced from a MW discharge of dilute (3%) CF_4 in Ar. Typical pressures of Ar and CF_4 gases in the discharge tube were 0.16–0.19 Torr (1 Torr = 133.3 Pa) and 5 mTorr, and those of C_2H_2, C_2D_2, and C_2H_4 were 16, 1, and 16 mTorr, respectively. The total pressure in the reaction zone was 0.19–0.20 Torr, when both MW(A) and MW(B) were operated.

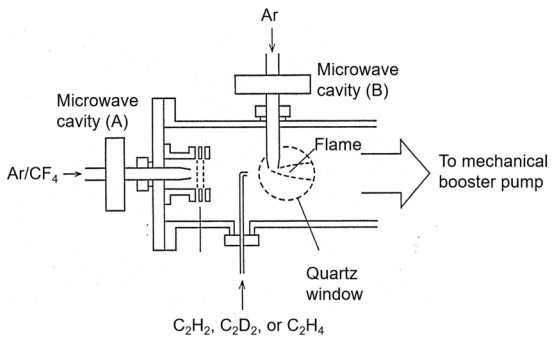

Fig. 1. The flowing afterglow apparatus for studying energy-transfer reactions from metastable Ar($^3P_2$) atoms to C_2H, C_2D, and C_2H_3 radicals.

3. Results and Discussion

3.1 Emission spectra and dissociative excitation processes

The minimum energies required for the formation of CH(A:v'=0–2) and CD(A:v'=0–2) from C_2H, C_2D, and C_2H_3 radicals are as follows.

$$C_2H \rightarrow CH(A:v'=0) + C - 10.57\ eV \quad (4a)$$
$$\rightarrow CH(A:v'=1) + C - 10.91\ eV \quad (4b)$$
$$\rightarrow CH(A:v'=2) + C - 11.22\ eV \quad (4c)$$

$$C_2D \rightarrow CD(A:v'=0) + C - 10.73\ eV \quad (5a)$$
$$\rightarrow CD(A:v'=1) + C - 10.98\ eV \quad (5b)$$
$$\rightarrow CD(A:v'=2) + C - 11.22\ eV \quad (5c)$$

$$C_2H_3 \rightarrow CH(A:v'=0) + CH_2 - 9.94\ eV \quad (6a)$$
$$\rightarrow CH(A:v'=1) + CH_2 - 10.28\ eV \quad (6b)$$
$$\rightarrow CH(A:v'=2) + CH_2 - 10.60\ eV \quad (6c)$$

Therefore, the formation of CH(A:v'=0–2) and CD(A: v' =0–2) from C_2H, C_2D, and C_2H_3 is energetically accessible.

$$Ar(^3P_2) + C_2H$$
$$\rightarrow CH(A:v'=0) + C + Ar + 0.98\ eV \quad (7a)$$
$$\rightarrow CH(A:v'=1) + C + Ar + 0.64\ eV \quad (7b)$$
$$\rightarrow CH(A:v'=2) + C + Ar + 0.33\ eV \quad (7c)$$

$$Ar(^3P_2) + C_2D$$
$$\rightarrow CD(A:v'=0) + C + Ar + 0.82\ eV \quad (8a)$$
$$\rightarrow CD(A:v'=1) + C + Ar + 0.57\ eV \quad (8b)$$
$$\rightarrow CD(A:v'=2) + C + Ar + 0.33\ eV \quad (8c)$$

$$Ar(^3P_2) + C_2H_3$$
$$\rightarrow CH(A:v'=0) + CH_2 + Ar + 1.61\ eV \quad (9a)$$
$$\rightarrow CH(A:v'=1) + CH_2 + Ar + 1.27\ eV \quad (9b)$$
$$\rightarrow CH(A:v'=2) + CH_2 + Ar + 0.95\ eV \quad (9c)$$

The heats of formation described above were calculated using reported thermochemical and spectroscopic data.[14,15)] Since the heat of formation of C_2D has not been reported, it was estimated to be 559.08 kJ/mol from reported dissociation energy of D–CCD (46754 cm^{-1})[16)] and heats of formation of C_2D_2 and D.[14)]

The following reactions are endoergic. Therefore, they cannot contribute to the

formation of CH(A:v'=0−2) and CD(A:v'=0−2) in the Ar afterglow reactions of C_2H_2 and C_2D_2.

$Ar(^3P_2) + C_2H_2$
→ CH(A:v'=0) + CH + Ar – 1.29 eV (10a)
→ CH(A:v'=1) + CH + Ar – 0.96 eV (10b)
→ CH(A:v'=2) + CH + Ar – 0.64 eV (10c)

$Ar(^3P_2) + C_2D_2$
→ CD(A:v'=0) + CD + Ar – 1.46 eV (11a)
→ CD(A:v'=1) + CD + Ar – 1.20 eV (11b)
→ CD(A:v'=2) + CD + Ar – 0.97 eV (11c)

On the other hand, the following reactions for C_2H_3 are exoergic, so that they are energetically accessible.

$Ar(^3P_2) + C_2H_4$
→ CH(A:v'=0) + CH_3 + Ar + 1.55 eV (12a)
→ CH(A:v'=1) + CH_3 + Ar + 1.21 eV (12b)
→ CH(A:v'=2) + CH_3 + Ar + 0.89 eV (12c)

Emission spectra were measured under three different conditions. Figures 2a, 2b, and 2c show emission spectra obtained by switching on both MW(A) and MW(B), only MW(B), and only MW(A), respectively. CH($A^2\Delta$–$X^2\Pi_r$) emission spectrum with rotational fine structures is observed in Fig. 2a, where strong stray ArI lines are partially overlapped. It is known that not only metastable $Ar(^3P_{0,2})$ atoms but also Ar^+, Ar_2^+, and Ar^{+*}(metastable ions) ions are generated by MW discharge of Ar in an Ar FA.[17-19] Suzuki and Kuchitsu[17] observed CH(A-X) emission system from the Ar afterglow reaction of C_2H_2, where MW was used for the generation of Ar active species. In their study, the CH(A-X) emission reduced its intensity by application of an electrostatic potential on the ion-collector grid placed between the discharge section and reaction zone. Based on this fact and energetics, they concluded that CH(A) is formed by the Ar^{+*}/C_2H_2 reaction. We examined the contribution of the Ar^{+*}/C_2H_2 reaction to the CH(A-X) emission by switching off MW(A). As shown in Fig. 2b, a weak CH(A-X) emission arising from the Ar^{+*}/C_2H_2 reaction is observed. The peak intensity of CH(A-X) in Fig. 2a and 2b is 1:0.33, indicating that the contribution of the Ar^{+*}/C_2H_2 reaction is 33% in Fig. 2a. Figure 2c was obtained by switching off MW(B), where weak emissions arising from stray light of MW(A) are observed. We obtained the CH(A-X) emission resulting from the $Ar(^3P_2)/C_2H$ reaction by subtracting the contribution of the Ar^{+*}/C_2H_2 reaction and stray light from MW(A), assuming that the CH(A-X) emission resulting from the Ar^{+*}/C_2H_2 reaction is unchanged by switching on or off MW(A). The result obtained is shown in Fig. 3a.

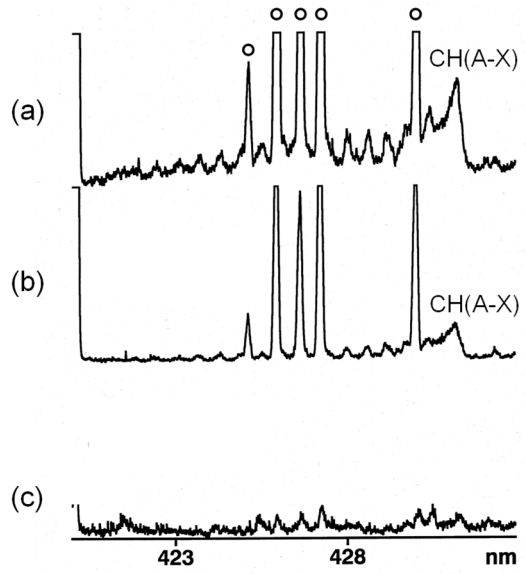

Fig. 2. Emission spectra obtained from (a) $Ar(^3P_2)/C_2H$ and Ar^{+*}/C_2H_2, (b) Ar^{+*}/C_2H_2, and (c) background emission from MW(A) in Fig. 1. Lines marked ○ are stray ArI lines.

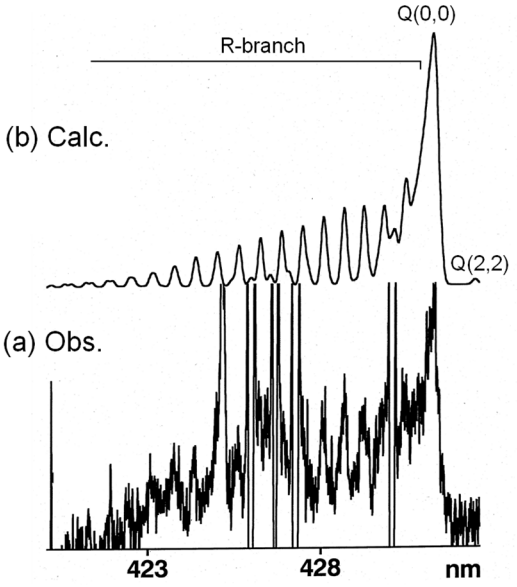

Fig. 3. (a) observed and (b) simulated emission spectra of CH($A^2\Delta$–$X^2\Pi_r$) band system from the $Ar(^3P_2)/C_2H$ reaction. The observed spectrum was obtained from spectra (a) – (b) – (c) in Fig. 2.

Figure 4a shows CD(A-X) emission spectrum obtained from the $Ar(^3P_{0,2})/C_2D$ reaction. This spectrum was obtained by subtracting the contribution of the Ar^{+*}/C_2D_2 reaction and stray light from MW(A), as in the case of the Ar^{+*}/C_2H reaction.

Figures 5a, 5b, and 5c show emission spectra obtained from $Ar(^3P_2)/C_2H_4$ + $Ar(^3P_2)/C_2H_3$ + Ar^{+*}/C_2H_4, $Ar(^3P_2)/C_2H_4$ + Ar^{+*}/C_2H_4, and background emission from MW(A), respectively. These emission spectra were observed by switching on both MW(A) and MW(B), only MW(B), and only MW(A), respectively. CH(A-X) emission is observed in Fig 5a, where strong stray ArI lines are partially overlapped. Weaker CH(A-X) emission is also observed in spectrum (b), indicating that $Ar(^3P_2)/C_2H_4$ + Ar^{+*}/C_2H_4 reactions give CH(A-X) emission. A comparison of peak intensity of CH(A-X) emission between Fig. 1a and Fig. 1b shows that the contribution of the $Ar(^3P_2)/C_2H_4$ + Ar^{+*}/C_2H_4 reactions to the CH(A-X) emission is 53%. This value was estimated assuming that the intensity of the CH(A-X) emission from the $Ar(^3P_2)/C_2H_4$ + Ar^{+*}/C_2H_4 reactions was independent of the switching on or off MW(A). The CH(A-X) emission from the $Ar(^3P_2)/C_2H_3$ reaction was obtained by subtracting the contribution of the $Ar(^3P_2)/C_2H_2$ + Ar^{+*}/C_2H_2 reactions and stray light from MW(A), assuming that the CH(A-X) emission resulting from the $Ar(^3P_2)/C_2H_4$ + Ar^{+*}/C_2H_4 reactions is unchanged by switching on or off MW(A). The result obtained is shown in Fig. 6a.

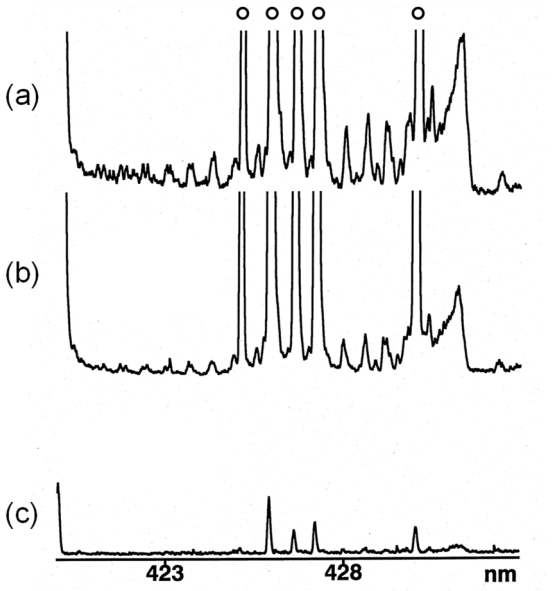

Fig. 5. Emission spectra obtained from (a) $Ar(^3P_2)/C_2H_4$ + $Ar(^3P_2)/C_2H_3$ + Ar^{+*}/C_2H_4, (b) $Ar(^3P_2)/C_2H_4$ + Ar^{+*}/C_2H_4, and (c) background emission from MW(A) in Fig. 1. Lines marked O are stray ArI lines.

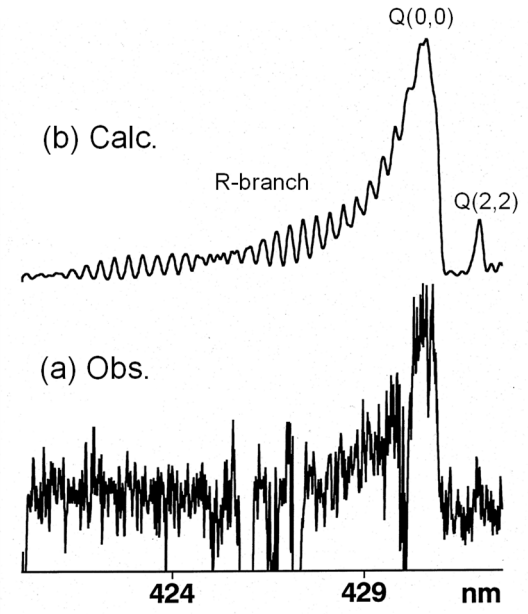

Fig. 4. (a) observed and (b) simulated emission spectra of $CD(A^2\Delta–X^2\Pi_r)$ band system from the $Ar(^3P_2)/C_2D$ reaction.

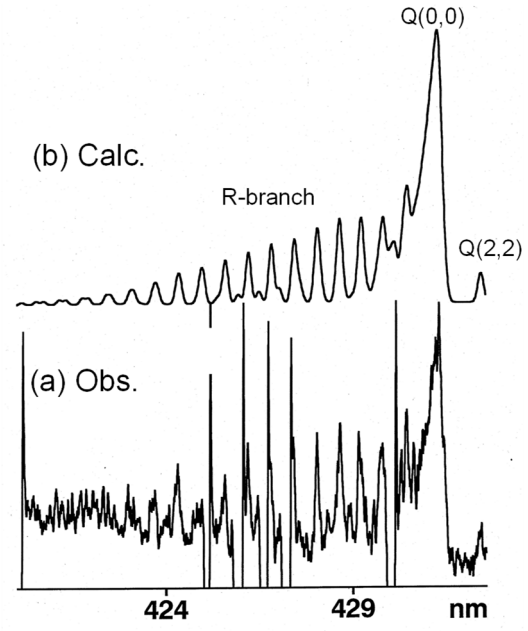

Fig. 6. (a) observed and (b) simulated emission spectra of $CH(A^2\Delta–X^2\Pi_r)$ band system from the $Ar(^3P_2)/C_2H_3$ reaction. The observed spectrum was obtained from spectra (a) – (b) – (c) in Fig. 5.

Table 1. Observed and prior vibrational distributions (%) of CH(A) and CD(A) produced from the reactions of $Ar(^3P_2)$ with C_2H, C_2D, and C_2H_3.

	C_2H			C_2D			C_2H_3		
v'	$N_{v'}$	$P^o_{v'}$ Processes (a)/(b)	$P^o_{v'}$ Process (c)	$N_{v'}$	$P^o_{v'}$ Processes (a)/(b)	$P^o_{v'}$ Process (c)	$N_{v'}$	$P^o_{v'}$ Process (d)	$P^o_{v'}$ Process (f)
0	100	100	100	100	100	100	100	100	100
1	25	53	28	25	57	33	25	24	17
2	1	19	4	6	26	7	4	4	2

Table 2. Observed rotational temperatures (K) of CH(A) and CD(A) produced from the reactions of $Ar(^3P_2)$ with C_2H, C_2D, and C_2H_3.

	C_2H	C_2D	C_2H_3
v'=0	1900	3800	1900
v'=1	1200	2400	1200
v'=2	300	600	800

3.3 Rovibrational distributions of CH(A: v' =0–2) and CD(A: v' =0–2) in the reactions of $Ar(^3P_2)$ with C_2H, C_2D, and C_2H_3 radicals

Rovibrational distributions of CH(A:v'=0–2) and CD(A:v'=0–2) in the $Ar(^3P_2)$/M (M = C_2H, C_2D, and C_2H_3) reactions were determined by a computer simulation of CH(A–X) and CD(A–X) bands. The simulation method used in this study was the same as that reported in our previous studies on CH_4,[5] C_2H_2,[6], and C_2D_2.[7] In Figs. 3b, 4b, and 6b are shown the best fit spectra of the CH(A–X) and CD(A–X) bands from C_2H, C_2D, and C_2H_3, calculated assuming single Boltzmann rotational distributions for each v' level. Vibrational distributions and rotational temperatures thus obtained are given in Tables 1 and 2. From the observed rovibrational distributions of CH(A) and CD(A), we evaluated the average vibrational and rotational energies of CH(A) and CD(A) states, denoted as $<E_v>$ and $<E_r>$, and average fractions of excess energies deposited into vibrational and rotational energies of CH(A) and CD(A), denoted as $<f_v>$ and $<f_r>$, respectively. In the $Ar(^3P_2)/C_2H$ and $Ar(^3P_2)/C_2D$ reactions, the average fractions of excess energies deposited into relative translational energy of neutral fragments, $<f_t>$, were estimated from the $<f_v>$ + $<f_r>$ values. Results obtained are summarized in Table 3. As discussed in our previous paper,[6-8] it is expected that the vibrational and rotational relaxation of CH(A) by collisions with the buffer rare gas is insignificant within their radiative lifetimes of about 500 ns for CH(A),[20,21] so that observed rovibrational distributions in the Ar FA reflect nascent distributions.

Table 3. Average vibrational and rotational energies (eV) deposited into CH(A) and average fractions of excess energies (%) deposited into vibration and rotation of CH(A) and CD(A) in the reactions of $Ar(^3P_2)$ with C_2H, C_2D, and C_2H_3.

C_2H	$<E_v>$	0.073
	$<E_r>$	0.15
	$<f_v>$	7.4
	$<f_r>$	15.4
	$<f_v>+<f_r>$	22.8
	$<f_t>$	77.2
C_2D	$<E_v>$	0.072
	$<E_r>$	0.29
	$<f_v>$	8.8
	$<f_r>$	35.5
	$<f_v>+<f_r>$	44.3
	$<f_t>$	55.7
C_2H_3	$<E_v>$	0.086
	$<E_r>$	0.15
	$<f_v>$	5.4
	$<f_r>$	9.3
	$<f_v>+<f_r>$	14.7

The following tendencies are found for the observed rovibrational distributions of CH(A) and CD(A).

(1) The vibrational population of CH(A:v'=0–2) and CD(A:v'=0–2) rapidly decrease with increasing v'. The N_1/N_0 ratio for the three reactions were the same (0.25), whereas the N_2/N_0 ratio decreases from

0.06 to 0.01 in the order of C_2D, C_2H_3, and C_2H.

(2) The rotational temperatures of CH(A:v'=0–2) and CD(A: v' =0–2) decrease with increasing v'. The rotational temperatures of CD(A:v'=0–2) from C_2D are higher than those of CH(A:v'=0–2) from C_2H by a factor of 2. The rotational temperatures of CH(A:v'=0–2) from C_2H_3 are similar to those from C_2H.

(3) There is no significant difference in the $<f_v>$ value between C_2H and C_2D, whereas the $<f_r>$ value of C_2D is larger that of C_2H by a factor of 2.3. The $<f_v>$ and $<f_r>$ values of C_2H_3 are smaller than those of C_2H and C_2D.

(4) The $<f_t>$ values of C_2H and C_2D are large (≥56%), indicating that most of excess energies are partitioned into relative translational energies of neutral CH(A) + C and CD(A) + C fragments. It is therefore reasonable to assume that CH(A) and CD(A) are formed through highly repulsive potentials.

3.4 The formation mechanisms of CH(A) and CD(A) from the reactions of Ar($^3P_2$) with C_2H, C_2D, and C_2H_3 radicals

3.4.1 Statistical models

The formation dynamics of CH(A) and CD(A) from the Ar($^3P_2$)/C_2H and Ar($^3P_2$)/C_2D reactions is discussed assuming two-body and three-body dissociation mechanisms, which have been used in the formation of CH($A^2\Delta$) from Ar($^3P_2$)/CH_3 and Ar($^3P_2$)/C_2H_5,[9,10] OH($A^2\Sigma^+$) from Ar($^3P_{0,2}$)/H_2O,[22] and NH($A^3\Pi_i$) from Ar($^3P_{0,2}$)/NH_3.[23] Possible processes for CH(A) are as follows. Similar processes can be applied to the formation of CD(A) from the Ar($^3P_2$)/C_2D reaction.

(a) Two-body dissociation process through resonant excitation transfer

$$\begin{aligned} &Ar^* + C_2H \rightarrow C_2H^* + Ar \\ &C_2H^* \rightarrow CH(A) + C \end{aligned} \quad (13)$$

(b) Two-body dissociation process through ion-pair formation

$$\begin{aligned} &Ar^* + C_2H \rightarrow Ar^+C_2H^- \rightarrow ArCH^* + C \\ &ArCH^* \rightarrow CH(A) + Ar \end{aligned} \quad (14)$$

(c) Three-body dissociation process through collision complex

$$\begin{aligned} &Ar^* + C_2H \rightarrow ArC_2H^{**} \\ &ArC_2H^{**} \rightarrow CH(A) + C + Ar \end{aligned} \quad (15)$$

In process (a), energy is resonantly transferred from Ar* to C_2H, and then C_2H^{**} dissociates into CH(A) + C. In processes (b) and (c), CH(A) is produced through collision complexes, ArCH* and ArC_2H^*, respectively. ArCH* originates from an ion-pair potential V(Ar^+–C_2H^-). In order to produce ArCH*, the ion-pair potential must be sufficiently low to couple with the entrance V(Ar*–C_2H) potential. Since the electron affinity of C_2H is relatively high (2.97 eV),[24] V(Ar^+–C_2H^-) potential is located just 1.24 eV above the entrance V(Ar*–C_2H) potential at dissociation limits. Therefore, the ion-pair potential is expected to be sufficiently low to interact strongly with the entrance potential. Thus, the second process cannot be excluded from the formation mechanism of CH(A).

Statistical vibrational and rotational distributions were calculated for the above three processes. According to a simple statistical theory,[25-27] the probability of forming a CH(A:v', N') rovibrational level and a CH(A:v') vibrational level through processes (a) and (b) is expressed by the same equation

$$P^o_{v'N'} \propto (2N'+1)(E_{\rm tot} - E_{v_{\rm CH^*}} - E_{r_{\rm CH^*}})^{1/2} \quad (16a)$$

$$P^o_{v'} \propto (E_{\rm tot} - E_{v_{\rm CH^*}})^{3/2}. \quad (16b)$$

On the other hand, that through process (c) is given by

$$P^o_{v'N'} \propto (2N'+1)(E_{\rm tot} - E_{v_{\rm CH^*}} - E_{r_{\rm CH^*}})^{2} \quad (17a)$$

$$P^o_{v'} \propto \left(E_{\rm tot} - E_{v_{\rm CH^*}}\right)^{3}. \quad (17b)$$

The prior vibrational and rotational distributions of CH(A: v'=0–2) calculated for processes (a)/(b) and (c) are compared with the observed ones in Table 1 and Figs. 7a–7c. The prior vibrational distribution of CH(A: v'=0–2) and rotational distributions of CH(A: v'=0–2) predict higher vibrational and rotational excitation than the observed ones for both two-body models (a)/(b) and three-body dissociation model (c).

The deviation from prior vibrational and rotational distributions can often be expressed in the form of surprisal,[27]

$$I_v = -\ln[P(v)/P^o(v)], = \lambda_0 + \lambda_v f_v \quad (18a)$$

$$I_R = -\ln[P(v,N)/P^o(v,N)] = \theta_0 + \theta_R g_N \quad (18b)$$

where $f_v = E_v/E_{tot}$, $g_N = E_N/(E_{tot}-E_v)$, $P(v) = N_{v'}$ and $P(v,N) = N_{v'N'}$.

Figure A1 in Appendix shows vibrational and rotational surprisal plots of CH(A: v' =0–2). When the two-body and three-body dissociation models for processes (a)/(b) and (c) are used for $P^o_{v'N'}$ and $P^o_{v'}$, good linear relationships are found in the surprisal plots of CH(A: v'=0–2) in the f_v and g_N range given in Table A1 in Appendix. These results imply that an exponential gap behavior is present between the experimental and statistical distributions in most cases. From slopes of each surprisal plot, positive vibrational and rotational surprisal parameters are obtained in all cases for the cases of C_2H (Table A1 in Appendix) because the observed vibrational and rotational distributions are lower than prior ones. The rotational surprisal parameter of CH(A: v'=0–2) increases with increasing v', in both processes (a)/(b) and (c), suggesting that the deviation from prior distribution increases with increasing v'.

The prior vibrational and rotational distributions of CD(A: v'=0–2) calculated for processes (a)/(b) and (c) are compared with the observed ones in Table 1 and Figs. 8a–8c. The prior vibrational distribution of CD(A: v'=0–2) for processes (a)/(b) is much higher than the observed one, whereas that for process (c) is slightly higher than the observed one (Table 1). The prior rotational distributions of CD(A: v' =0–2) for process (a)/(b) are much higher than observed ones. On the other hand, a reasonable agreement is found between prior rotational distributions of CD(A: v' =0,1) for process (c) for low N' levels below N' ≈15,

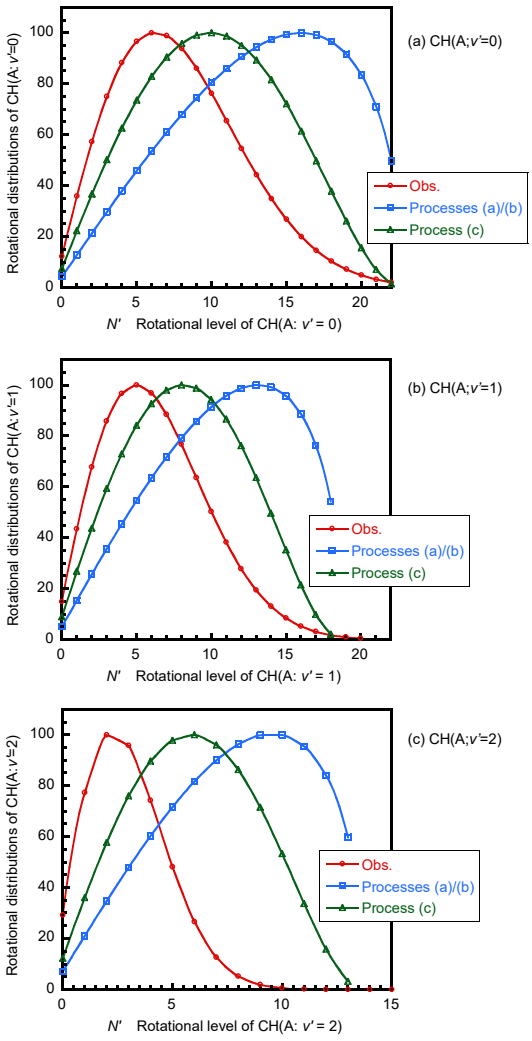

Fig. 7. Observed and two-body and three-body prior rotational distributions of CH(A: v'=0–2) in the Ar($^3P_2$)/C_2H reaction.

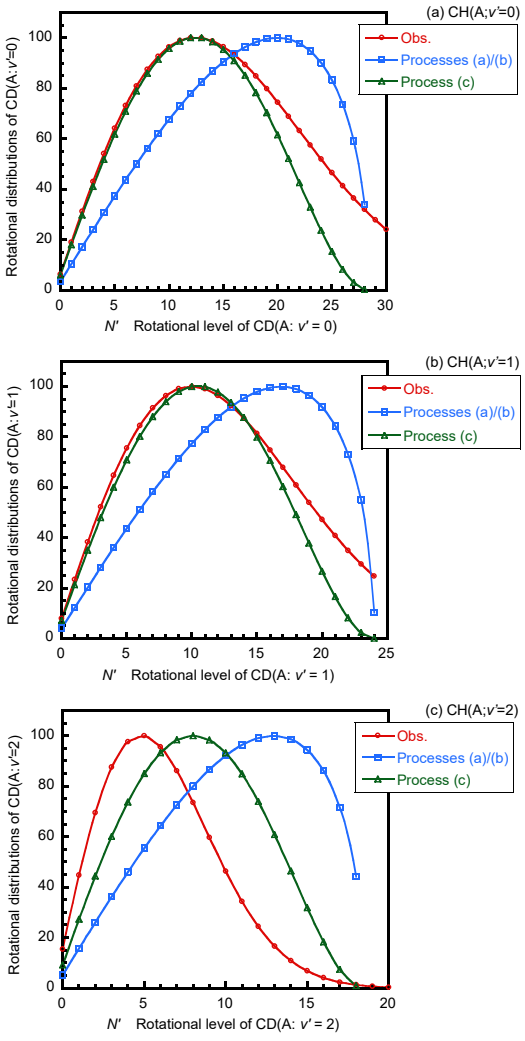

Fig. 8. Observed and two-body and three-body prior rotational distributions of CD(A: v'=0–2) in the Ar($^3P_2$)/C_2D reaction.

whereas the prior rotational distribution of CD(A: v'=2) for process (c) is higher than the observed one.

Figure A2 in Appendix shows vibrational and rotational surprisal plots of CD(A: v' =0–2). When the two-body and three-body dissociation models for processes (a)/(b) and (c) are used for $P^o_{v'N'}$ and $P^o_{v'}$, good linear relationships are found in the surprisal plots of CD(A: v'=0–2) in the f_v and g_N range given in Table A1 in Appendix. The vibrational surprisal parameter of CD(A: v' =0–2) for processes (a)/(b) gave a positive value (2.5) because the observed vibrational distribution is lower than that expected from prior one. On the other hand, the vibrational surprisal parameter for process (c) (0.18) is small, suggesting that there is no significant difference between the observed and prior distributions. The rotational surprisal parameters for CD(A: v' =0–2) for processes (a)/(b) are positive because the observed rotational distributions are lower than those expected from prior ones. The rotational surprisal parameters for CD(A: v' =0,1) for process (c) are small negative values (−0.50 and −0.38), suggesting that the observed rotational distributions are slightly higher than those expected from prior ones. The rotational surprisal parameter of CD(A: v'=2) is positive (3.3), indicating that the observed distribution is lower than the prior one. The rotational surprisal parameter of CD(A: v'=0–2) increases with increasing v', in both processes (a)/(b) and (c), suggesting that the deviation from prior distribution increases with increasing v'.

It should be noted that deviations of observed vibrational and rotational distributions of C_2H and C_2D from prior ones for three-body process (c) are smaller than those for two-body processes (a) and (b). Therefore, three-body processes are more favorable if energy-transfer processes are governed by statistical models. Vibrational and rotational surprisal parameters obtained for C_2D are smaller than those for C_2H, indicating that deviations from prior distributions are small for the case of C_2D.

The following three processes may be responsible for the production of CH(A) from the Ar($^3P_2$)/C_2H_3 reaction.

(d) Two-body dissociation process through resonant excitation transfer

$$\begin{aligned} &Ar^* + C_2H_3 \rightarrow C_2H_3^{**} + Ar \\ &C_2H_3^{**} \rightarrow CH(A) + CH_2 \end{aligned} \quad (19)$$

(e) Two-body dissociation process through ion-pair formation

$$\begin{aligned} &Ar^* + C_2H_3 \rightarrow Ar^+C_2H_3^- \rightarrow ArCH^* + CH_2 \\ &ArCH^* \rightarrow CH(A) + Ar \end{aligned} \quad (20)$$

(f) Three-body dissociation process through collision complex

$$\begin{aligned} &Ar^* + C_2H_3 \rightarrow ArC_2H_3^* \\ &ArC_2H_3^* \rightarrow CH(A) + CH_2 + Ar \end{aligned} \quad (21)$$

The electron affinity of C_2H_3 is small (0.667 eV),[14] $V(Ar^+–C_2H_3^-)$ potential is located 3.54 eV above the entrance $V(Ar^*–C_2H_3)$ potential at dissociation limits. Therefore, the ion-pair potential is too high to interact strongly with the entrance potential at a long distance between Ar* and C_2H_3. Thus, it is reasonable to assume that the ion-pair process (e) is not important compared with the case of C_2H. Thus, process (e) was excluded from possible processes in this study.

The probability of forming a CH (A: v', N') rovibrational level and a CH(A:v') vibrational level through process (d) is expressed by the equation

$$P^o_{v'N'} \propto (2N'+1)(E_{\mathrm{tot}} - E_{v_{\mathrm{CH}^*}} - E_{r_{\mathrm{CH}^*}})^5 \quad (22a)$$

$$P^o_{v'} \propto \left(E_{\mathrm{tot}} - E_{v_{\mathrm{CH}^*}}\right)^6. \quad (22b)$$

On the other hand, that through process (f) is given by

$$P^o_{v'N'} \propto (2N'+1)(E_{\mathrm{tot}} - E_{v_{\mathrm{CH}^*}} - E_{r_{\mathrm{CH}^*}})^{6.5} \quad (23a)$$

$$P^o_{v'} \propto \left(E_{\mathrm{tot}} - E_{v_{\mathrm{CH}^*}}\right)^{7.5}. \quad (23b)$$

The prior vibrational distribution of CH(A: v'=0–2) and rotational distributions of CH(A: v'=0–2) calculated for processes (d) and (f) are compared with the observed ones in Table 1 and Figs. 9a–9c. Surprisal plots and surprisal parameters obtained for CH(A) from C_2H_3 are given in Figure A3 and Table A1 in Appendix. Although a good agreement is observed between the prior vibrational distribution and observed one for process (d), the prior vibrational distribution of CH(A: v'=0–2) for process (f) is lower than the observed one. The prior rotational distribution of CH(A: v' =0–2) for processes (d) and (f) predict higher vibrational and rotational excitation than the observed ones for both two-body model (d) and three-body dissociation

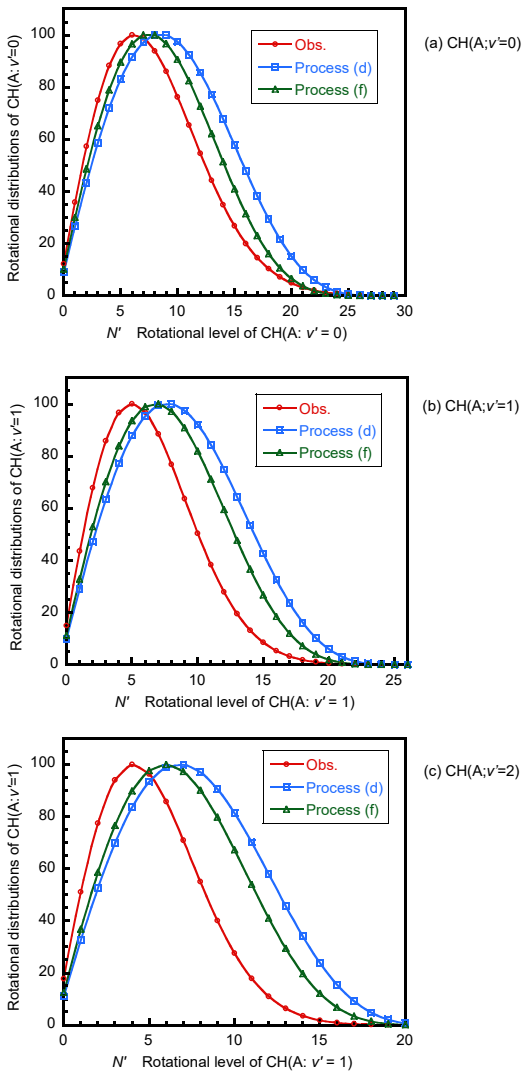

Fig. 9. Observed and two-body and three-body prior rotational distributions of CH(A: v'=0–2) in the Ar($^3P_2$)/C_2H_3 reaction.

model (f). The rotational surprisal parameter of CH(A: v'=0–2) increases with increasing v', in both processes (d) and (f), suggesting that the deviation from prior distributions increases with increasing v', as in the cases of C_2H and C_2D. The deviation of observed vibrational distribution of CH(A) from prior one for two-body process (d) is smaller than that for three-body process (f). On the other hand, deviations of observed rotational distributions of CH(A: v'=0–2) from prior ones for two-body process (d) are larger than those for three-body process (f).

3.4.2 Dissociative excitation process

In general, energy transfer from metastable rare gas atoms to molecules proceeds through near-resonant processes, where spin-conservation rule holds between reactants and products.[11,28-31] Therefore, it is likely that C_2H, C_2D, and C_2H_3 radicals are initially excited into near-resonant doublet and/or quartet states at the energy of Ar($^3P_2$:11.55 eV) because the ground states of theses radicals and CH(A) are both doublets and the ground state of carbon atom is ^3P. The ionization potentials (IPs) of C_2H, C_2D, are C_2H_3 were measured as 11.61, 11.58, and 8.25 eV, respectively.[14,32] Here, IP of C_2D was estimated from reported appearance potential of C_2D^+ under electron-impact ionization and dissociation energy of D(D–CCD).[14,32] The IPs of C_2H and C_2D are slightly higher than the energy of Ar($^3P_2$:11.55 eV), whereas that of C_2H_3 is lower than the energy of Ar($^3P_2$). It is therefore reasonable to assume that precursor states for C_2H and C_2D are not superexcited states above their first IPs, whereas that for C_2H_3 is superexcited state located above first IP of C_2H_3. In the Ar($^3P_2$)/C_2H reactions, most probable precursor states are doublet and/ or quartet Rydberg states converging to the ground ionic states of C_2H. According to *ab initio* calculations by Koures and Harding,[33] many doublet and quartet Rydberg states exist below first IP for C_2H. Some of them will be precursor states. Higher energy deposition into rotation than into vibration even though the ground state of C_2H is linear[34] suggests that bending modes of precursor C_2H** Rydberg states are excited after energy transfer.

Analogous Rydberg states will exist for C_2D below its IP. It is therefore expected that the formation of CD(A) from the Ar($^3P_2$)/C_2D reaction proceeds though similar Rydberg states converging to the ground state of C_2D^+. A higher rotational excitation of CD(A) than CH(A) is explained by larger torque in CD(A) after dissociation of C_2D** due to larger moment of inertia. The high position of excess energies into translational energies of CH(A) + C and CD(A) + C indicates that CH(A) and CD(A) are formed through curve crossing between precursor Rydberg states and highly repulsive CH(A) + C and CD(A) + C potentials.

The formation of CH(A) from C_2H_3 probably proceeds through superexcited states above the first IP of C_2H_3. Unknown Rydberg states of C_2H_3** converging to excited ionic states of $C_2H_3^+$ are possible precursor states leading to CH(A) + CH_2. Although excess energies in the Ar($^3P_2$)/C_2H_3 reaction are larger than those in the Ar($^3P_2$)/C_2H reaction, no significant enhancement of deposition of excess energy

into vibration and rotation of CH(A) was observed. Since the degree of freedom of CH_2 fragment is much larger than C from the $Ar(^3P_2)/C_2H$ reaction, CH_2 can accept more excess energy after reaction. This will be one reason for the low energy deposition of excess energy into vibration and rotation of CH(A) in the $Ar(^3P_2)/C_2H_3$ reaction.

We found that the observed vibrational and rotational distributions are lower than statistical two-body and three-body dissociation models in most cases. One reason may be the fact that lifetimes of intermediate states are too short to randomize excess energies into all degrees of freedom. Another reason may be the fact that electronic structures and molecular structures of precursor Rydberg states and repulsive potential curves leading to CH(A) and CD(A) play more important role in their decomposition processes.

4. Summary and Conclusion

Dissociative excitation of C_2H, C_2D, and C_2H_3 radicals by collisions with metastable $Ar(^3P_2)$ atoms has been studied by observing CH(A-X) and CD(A-X) emissions in the Ar FA. The nascent vibrational and rotational distributions of CH(A:v'=0–2) and CD(A:v'=0–2) were determined from spectral simulation. The vibrational distributions of CH(A) and CD(A) rapidly decreased with increasing v' in all reactions. The rotational distributions of CH(A:v'=0–2) and CD(A:v'=0–2) states were expressed by single Boltzmann temperatures of 300–1900 K and 600–3800 K, respectively. In most cases, the observed vibrational and rotational distributions are lower than statistical prior ones obtained by assuming two-body and three-body dissociation models. In the $Ar(^3P_2)/C_2H$ and $Ar(^3P_2)/C_2D$ reactions, more excess energies are deposited into rotational modes than into vibrational ones of CH(A) and CD(A). Taking account of the linear C_2H and C_2D molecules in the ground states, we concluded that rotational excitation of CH(A) and CD(A) arises from excitation of bending modes of precursor C_2H^{**} and C_2D^{**} Rydberg states. It was found that most of excess energy (≥56%) is deposited into relative translational energies of CH(A) + C and CD(A) + C products Therefore, we concluded that CH(A) and CD(A) are formed through highly repulsive potentials.

Acknowledgments

This work was supported by the Mitsubishi foundation (1996) and JSPS KAKENHI Grant number 09440201 (1997-2000).

References

1) N. Mutsukura and K. Miyatani, *Diamond Relat. Mater.*, 4, 342 (1995).
2) P. Yang , S. C. H . Kwok, R. K. Y. Fu , Y. X. Leng, J. Wang, G. J. Wan, N. Huang, Y. Leng, and P. K. Chu, *Surf. Coat. Tech.*, 177/178, 747 (2004).
3) S. Avtaeva and V. Gorokhovsky, *Plasma Chem. Plasma Process.*, 41, 815 (2021).
4) M. Tsuji, K. Kobarai, H. Obase, H. Kouno, and Y. Nishimura, *J. Chem. Phys.*, 94, 277 (1991).
5) M. Tsuji, T. Komatsu, M. Tanaka, M. Nakamura, Y. Nishimura, and H. Obase, *Chem. Lett.*, 26, 359 (1997).
6) M. Tsuji, T. Komatsu, K. Uto, J.-I. Hayashi, and T. Tsuji, *Eng. Sci. Rep., Kyushu Univ.*, 43, 8 (2021).
7) M. Tsuji, T. Komatsu, K. Uto, J.-I. Hayashi, and T. Tsuji, *Eng. Sci. Rep., Kyushu Univ.*, 43, 23 (2021).
8) M. Tsuji, T. Komatsu, K. Uto, J.-I. Hayashi, and T. Tsuji, *Eng. Sci. Rep., Kyushu Univ.*, 43, 1 (2022).
9) M. Tsuji, H. Kouno, Y. Nishimura, H. Obase, and K. Kasatani, *J. Chem. Phys.*, 95, 7317 (1991).
10) M. Tsuji, H. Kouno, H. Ujita, and Y. Nishimura, *J. Chem. Phys.*, 96, 6746 (1992).
11) J M. Tsuji, K. Kobarai, and Y. Nishimura, *J. Chem. Phys.*, 93, 3133 (1990).
12) *NIST Chemical Kinetics Database*, Standard Reference Database 17, Version 7.0 (Web Version), Release 1.6.8., Data Version 2015.09, and references therein.
13) J. Berkowitz, C. A. Mayhew, and B. Ruščić, *J. Chem. Phys.*, 88, 7396 (1988).
14) *NIST Chemistry WebBook*, NIST Standard Reference Database, Number 69 (2018): http://webbook.nist.gov/chemistry.
15) K. P. Huber and G. Herzberg, "*Molecular Spectra and Molecular Structure, IV. Constants of Diatomic Molecules*", Van Nostrand Reinhold, New York (1979).
16) S. H. S. Wilson, C. L. Reed, D. H. Mordaunt, M. N. R. Ashfold, amd M. Kawasaki, *Bull. Chem. Soc. Jpn.*, 69, 71 (1996).
17) K. Suzuki and K. Kuchitsu, *J. Photochem.*, 10, 401 (1979).
18) H. Obase, M. Tsuji, and Y. Nishimura, *Chem. Phys.*, 87, 93 (1984).
19) M. Endoh, M. Tsuji, and Y. Nishimura, *Chem. Phys. Lett.*, 109, 35 (1984).
20) J. Carozza and R. Anderson, *J. Opt. Soc. Amer.*, 67, 118 (1977).
21) M. Ortiz and J. Campos, *Physica B+C*, 114, 135 (1982).
22) H. L. Snyder, B. T. Smith, T. P. Parr, and R. M. Martin, *Chem. Phys.*, 65, 397 (1982).
23) H. Sekiya, N. Nishiyama, M. Tsuji, and Y. Nishimura, *J. Chem. Phys.*, 86, 163 (1987).
24) T. R. Taylor, C. Xu, and D. M. Neumark, *J. Chem. Phys.*,108, 10018 (1998).
25) R. D. Levine and J. L. Kinsey, "*Atom-Molecule Collision Theory*", ed. by R. B. Bernstein, Plenum, New York (1979), p. 693.
26) R. B. Bernstein, "*Chemical Dynamics via Molecular Beam and Laser Techniques*", Oxford University Press (1982).

27) R. D. Levine, *Bull. Chem. Soc. Jpn.*, 61, 29 (1988).
28) M. Tsuji, K. Kobarai, S. Yamaguchi, H. Obase, K. Yamaguchi, and Y. Nishimura, *Chem. Phys. Lett.*, 155, 481 (1989).
29) M. Tsuji, K. Kobarai, S. Yamaguchi, and Y. Nishimura, *Chem. Phys. Lett.*, 158, 470 (1989).
30) M. Tsuji, K. Kobarai, S. Yamaguchi, H. Obase, and Y. Nishimura, *Chem. Phys. Lett.*, 166, 485 (1990).
31) M. Tsuji, K. Kobarai, H. Kouno, H. Obase, and Y. Nishimura, *Jpn. J. Appl. Phys.*, 30, 862 (1991).
32) M. Davister and R. Locht, *Chem. Phys.*, 189, 805 (1994).
33) A. G. Koures and L. B. Harding, *J. Phys. Chem.*, 95, 1035 (1991).
34) R. Tarroni and S. Carter, *J. Chem. Phys.* 119, 12878 (2003).

Appendix

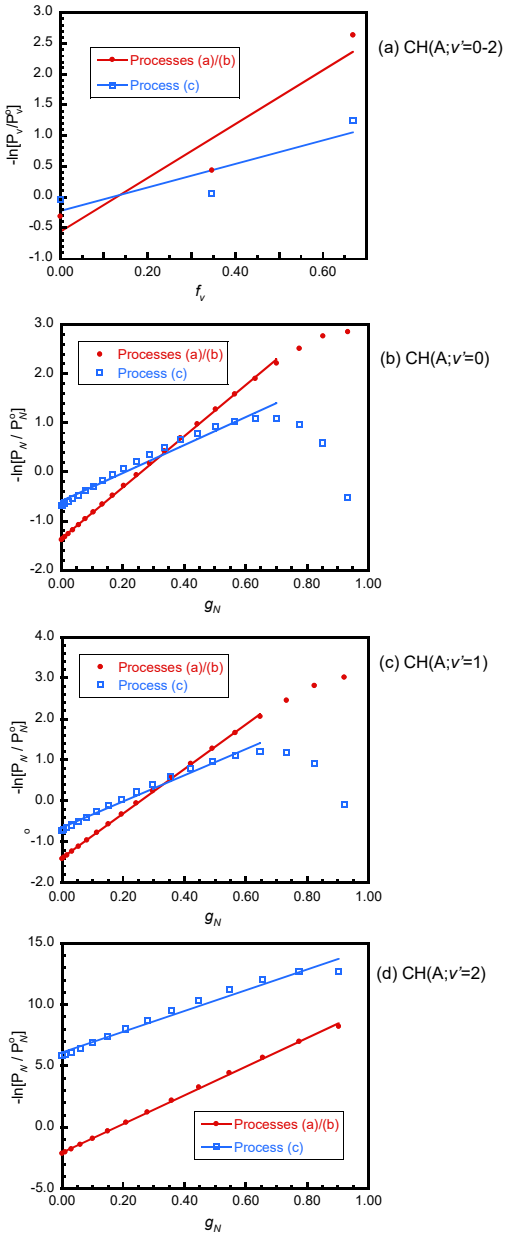

Fig. A1. Vibrational and rotational surprisal plots of CH(A: v' =0–2) in the Ar(^{3}P$_2$)/C$_2$H reaction.

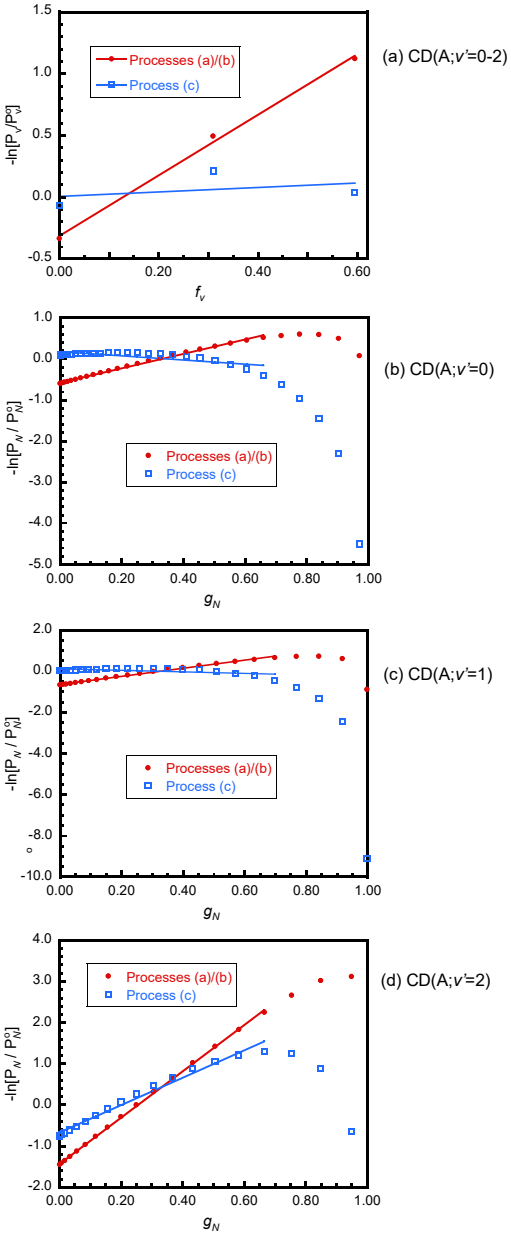

Fig. A2. Vibrational and rotational surprisal plots of CD(A: v' =0–2) in the Ar(^{3}P$_2$)/C$_2$D reaction.

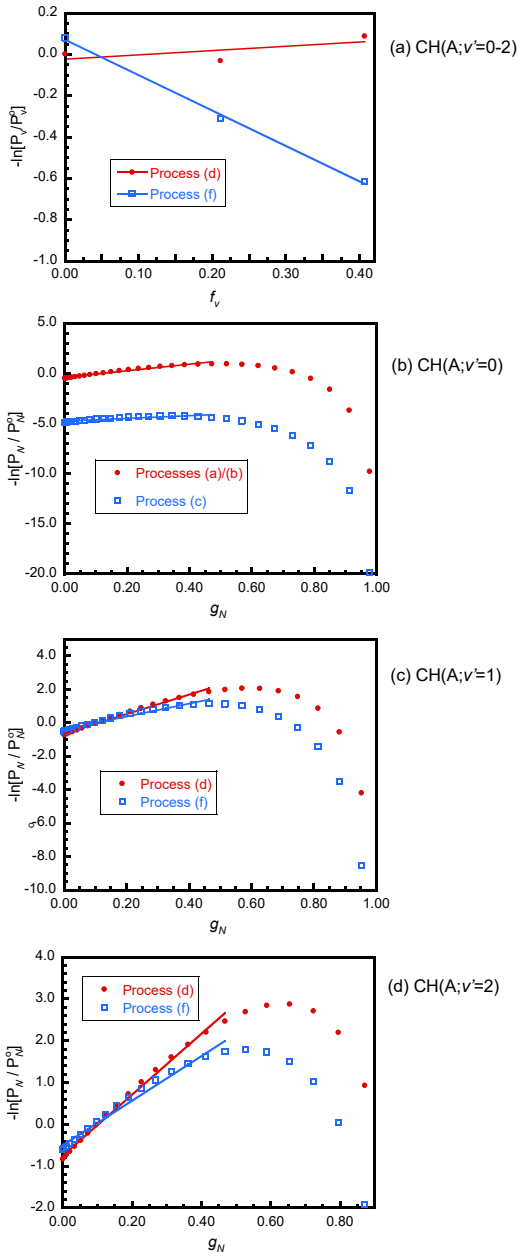

Fig. A3. Vibrational and rotational surprisal plots of CH(A: v' =0–2) in the Ar($^3P_2$)/C_2H_3 reaction.

Table A1. Vibrational and rotational surprisal parameters for CH(A) and CD(A) produced from the reactions of $Ar(^3P_2)$ with C_2H, C_2D, and C_2H_3.

		Vibrational surprisal parameter		Rotational surprisal parameter		f_v or g_N range
		Two-body processes (a)/(b)	Three-body process (c)	Two-body processes (a)/(b)	Three-body process (c)	
C_2H	CH(A: v'=0-2)	4.4	1.9			$f_v \leq 0.67$
	CH(A: v'=0)			5.2	2.8	$g_N \leq 0.7$
	CH(A: v'=1)			5.4	3.2	$g_N \leq 0.65$
	CH(A: v'=2)			8.5	11.7	$g_N \leq 0.90$
C_2D	CD(A: v'=0-2)	2.5	0.18			$f_v \leq 0.60$
	CD(A: v'=0)			1.8	−0.50	$g_N \leq 0.66$
	CD(A: v'=1)			2.0	−0.38	$g_N \leq 0.7$
	CD(A: v'=2)			5.6	3.3	$g_N \leq 0.67$
		Two-body process (d)	Three-body process (f)	Two-body process (d)	Three-body process (f)	
C_2H_3	CH(A: v'=0-2)	0.21	−1.7			$f_v \leq 0.41$
	CH(A: v'=0)			3.3	1.4	$g_N \leq 0.47$
	CH(A: v'=1)			5.8	3.9	$g_N \leq 0.46$
	CH(A: v'=2)			7.3	5.3	$g_N \leq 0.47$